Physical Communication 53 (2022) 101742

Contents lists available at ScienceDirect

Physical Communication

journal homepage: www.elsevier.com/locate/phycom

Error rates of arbitrary order optical wireless pulse-position modulation: An efficient approach

Konstantinos Yiannopoulos *, Nikos C. Sagias, Anthony C. Boucouvalas [1]

Department of Informatics and Telecommunications, University of Peloponnese, Akadimaikou G.K. Vlachou, 22131 Tripoli, Greece

A R T I C L E I N F O

Article history:
Received 17 January 2022
Received in revised form 20 April 2022
Accepted 5 May 2022
Available online 13 May 2022

Keywords:
Optical amplification
Pulse position modulation
Bit-error probability
Atmospheric scintillation
Pointing errors

A B S T R A C T

We present analytical results on the bit-error probability (BEP) of arbitrary order pulse-position modulation (PPM) of optically pre-amplified receivers. We use the Laguerre photon counting distribution so as to model the statistic of the optical noise, in order to accurately model the effects of signal and spontaneous noise beating at the optical detector. The great advantage of our proposed results is that they are exact and only require a finite summation over the optical noise modes and the modulation order. In addition, this approach enables the efficient calculation of the BEP in optical wireless communication links, under the presence of atmospheric scintillations and pointing errors.

1. Introduction

The utilization of optical beams in high capacity outdoor communication links has received significant attention [1–4], with a recent intense focus on space communications to the Moon [5,6]. The related demonstration prototypes utilize optical amplification and pulse-position modulation (PPM) with a goal to improve the receiver sensitivity [7,8], since the optical beams experience heavy transmission losses in outdoor environments. PPM is particularly appealing, as it provides a straight-forward trade-off between the bit-error probability (BEP) and the required bandwidth. The main body of the existing literature has addressed the BEP performance of PPM assuming Gaussian and Poisson noise statistics [9–13], that do not accurately describe the impact of the amplified spontaneous emission (ASE) in preamplified receivers. In receivers with optical pre-amplification, the signal-ASE and ASE-ASE beating noise terms dominate, and the noise is more accurately modeled by the χ^2 [14–16] or the Laguerre photon-counting distribution [17–19].

The main challenge that arises, when the Laguerre distribution is applied in preamplified systems, is related to high photon counts that are observed at the output of the optical amplifiers. In principle, the BEP of PPM can be numerically evaluated via an infinite sum over the Laguerre distribution. However, this approach becomes more time consuming as the photon counts increase, since a large number of terms need to be added in order to converge. This is the case when high gain amplifiers and/or wide bandwidth optical filters are employed. A more efficient approach is to convert the infinite sum into a finite one, but existing works are only limited to binary order PPM [14,18]. It is to be noted that the applicability of the binary PPM is limited by the fact that its error performance is worse than the on–off keying [14], while it simultaneously requires twice as much bandwidth. As a result, focus has shifted to higher order PPM modulations [8] and this is the topic of our work.

In the current work, we present novel analytical expressions for the BEP of an optically pre-amplified PPM receiver, where the Laguerre noise distribution is considered. Specifically, we present an expression for the BEP, that is in the form of a finite sum over the PPM order and the noise modes entering the optical receiver. The proposed expression is exact and the derived BEP numerical results fully coincide with equivalent results that are obtained via infinite summation. The advantage of our proposed expression is that it can be further used in order to assess the average BEP (ABEP) performance, when random losses are introduced, as is the case of fading and pointing errors in outdoor transmission systems. We show in the following sections that a finite summation is only required in these scenarios, as well. This approach reduces significantly the time that is required for the ABEP calculations in comparison with infinite summation, while simultaneously achieving the same degree of accuracy. To the best of our knowledge, this is the first time that such an analytical study is presented for arbitrary order PPM systems with or without fading and pointing errors. Within this context,

* Corresponding author.
E-mail address: kyianno@uop.gr (K. Yiannopoulos).

[1] Prof. Boucouvalas passed away on 28/10/2021. He contributed to the derivation of the analytical results in this work and provided useful comments and insights during the preparation of the initial versions of this manuscript.

https://doi.org/10.1016/j.phycom.2022.101742
1874-4907/

the current work could be of importance for the design and BEP evaluation of future communication systems that utilize higher modulation orders.

The rest of the paper is structured as follows: In Section 2 we present an analytical expression for the BEP performance of PPM receivers and demonstrate its accuracy. The analytical expression is then utilized in Section 3 to address the impact of fading on the ABEP. We present results on weak, moderate and strong fading for the Malaga-$\mathcal{M}$, $\gamma-\gamma$ and negative exponential distributions, and also calculate the performance improvement that can be achieved using spatial diversity. Finally, in Section 4 we include pointing errors in our analysis and show that the receiver performance is affected strongly by the beam-width. We also present results for the optimal beam-width that minimizes the ABEP in weak fading.

2. Q-PPM bit error probability

We consider a $Q-$ary PPM optical communication system, where each transmitted PPM symbol is encoded into Q successive time-slots. Each time only one of the slots contains the entirety of the symbol photons μ_s, while all slots are corrupted by optical noise that is distributed over M modes with each mode contributing λ photons. The received photons are converted into an electrical current via direct detection, and at each slot the detector generates photoelectrons, whose number depends on the instantaneous signal and noise energy levels. During a PPM slot that contains signal photons, the photon count n_1 is generated from the incident signal and noise photons, and n_1 follows the Laguerre distribution [17,18]

$$p_1\left(n_1,\mu_s,M\right)=\epsilon^M\,y^{n_1}\,\mathrm{e}^{-\epsilon\,\mu_s}\,L_{n_1}^{M-1}\left(x\right)\;,\tag{1}$$

where $y=\lambda/(1+\lambda)$, $\epsilon=1-y$, $x=-\epsilon^2\,\mu_s/y$ and $L_{n_1}^{M-1}\left(\cdot\right)$ stands for the associated Laguerre polynomial [20, eq. (8.970/1)]. During a slot that does not contain signal photons, the detector generates a photon count n_0 from the noise photons only, and the distribution simplifies, with respect to (1), to

$$p_0\left(n_0,M\right)=\epsilon^M\,y^{n_0}\binom{n_0+M-1}{n_0}.\tag{2}$$

The PPM demodulator monitors the random photon counts of the Q slots and makes a decision about the transmitted symbol using soft-decision decoding [21]. As a result, the symbol is determined from the slot with the highest count. Assuming that errors from equal counts cannot be resolved, a decision is correct when $n_1>\max\{n_0\}$. The corresponding probability equals [22, Eq. (8)]

$$P_{c,s}=\sum_{n=0}^{\infty}\left[F_0\left(n,M\right)\right]^{Q-1}\,p_1\left(n+1,\mu_s,M\right)\;,\tag{3}$$

where $F_0\left(n,M\right)$ denotes the cumulative distribution function of the photon count that is received in the absence of the signal

$$F_0\left(n,M\right)=P\left(n\geq n_0\right)=\sum_{n_0=0}^{n}p_0\left(n_0,M\right)\;.\tag{4}$$

2.1. The key result

The infinite sum that appears in (3) is evaluated from the generating function of the Laguerre polynomials [20, eq. (8.975/1)] via the following inverse z-transforms

$$F_0\left(n,M\right)=\epsilon^M\,\frac{1}{2\pi\jmath}\oint_{\mathcal{C}_\alpha}\frac{1}{(1-y\,z)^M\,(1-z)\,z^{n+1}}\,dz,\tag{5}$$

and

$$p_1\left(n+1,\mu_s,M\right)=\epsilon^M\,\mathrm{e}^{-\epsilon\,\mu_s}\,\frac{1}{2\pi\jmath}\oint_{\mathcal{C}_\beta}\frac{\exp(-\frac{y\,z}{1-y\,z}\,x)}{(1-y\,z)^M\,z^{n+2}}\,dz\,.\tag{6}$$

$\mathcal{C}_\alpha$ is a contour of integration that encloses the origin, but not the poles at $z=1$ and $z=1/y$, while contour $\mathcal{C}_\beta$ also encloses the origin but not the pole at $z=1/y$.

By substituting (5) and (6) in (3), the probability of a correct decision is evaluated from the multi-dimensional integral

$$\begin{aligned}P_{c,s}&=\frac{\epsilon^M\,\mathrm{e}^{-\epsilon\,\mu_s}}{(2\pi\jmath)^Q}\sum_{n=0}^{\infty}\oint_{\mathcal{C}_\alpha,\ldots,\mathcal{C}_\beta}\frac{\exp(-\frac{y\,z_Q}{1-y\,z_Q}\,x)\,dz_Q}{(1-y\,z_Q)^M\,z_Q^{n+2}}\prod_{q=1}^{Q-1}\frac{\epsilon^M\,dz_q}{(1-y\,z_q)^M\,(1-z_q)\,z_q^{n+1}}\\&=\underbrace{\frac{\epsilon^M\,\mathrm{e}^{-\epsilon\,\mu_s}}{(2\pi\jmath)^Q}\oint_{\mathcal{C}_\alpha,\ldots,\mathcal{C}_\beta}\frac{\exp(-\frac{y\,z_Q}{1-y\,z_Q}\,x)}{(1-y\,z_Q)^M\,z_Q}\left[\prod_{q=1}^{Q-1}\frac{\epsilon^M}{(1-y\,z_q)^M\,(1-z_q)}\right]\frac{\prod_{q=1}^{Q}dz_q}{\prod_{q=1}^{Q}z_q-1}}_{I}\,,\end{aligned}\tag{7}$$

with the constraint that $\prod_{q=1}^{Q}|z_q|>1$ for the summation to converge. We utilize partial fraction decomposition [20, eq. (2.102)]

$$\frac{\epsilon^M}{(1-y\,z_q)^M\,(1-z_q)}=\frac{1}{1-z_q}-\frac{y}{\epsilon}\sum_{m_q=0}^{M-1}\frac{\epsilon^{m_q+1}}{(1-y\,z_q)^{m_q+1}}\tag{8}$$

to evaluate I as

$$\begin{aligned}I&=\frac{1}{(2\pi\jmath)^Q}\oint_{\mathcal{C}_\alpha,\ldots,\mathcal{C}_\beta}\frac{\exp(-\frac{y\,z_Q}{1-y\,z_Q}\,x)}{(1-y\,z_Q)^M\,z_Q}\\&\quad\times\prod_{q=1}^{Q-1}\left[\frac{1}{1-z_q}-\frac{y}{\epsilon}\sum_{m_q=0}^{M-1}\frac{\epsilon^{m_q+1}}{(1-y\,z_q)^{m_q+1}}\right]\frac{\prod_{q=1}^{Q}dz_q}{\prod_{q=1}^{Q}z_q-1}\\&=\sum_{i=0}^{Q-1}\binom{Q-1}{i}\left(-\frac{y}{\epsilon}\right)^i\,I_i\,,\end{aligned}\tag{9}$$

where I_i $(i=0,\,1,\ldots,Q-1)$ corresponds to the integral

$$\begin{aligned}I_i&=\frac{1}{(2\pi\jmath)^Q}\oint_{\mathcal{C}_\alpha,\ldots,\mathcal{C}_\beta}\frac{\exp(-\frac{y\,z_Q}{1-y\,z_Q}\,x)}{(1-y\,z_Q)^M\,z_Q}\\&\quad\times\left[\prod_{q=1}^{i}\sum_{m_q=0}^{M-1}\frac{\epsilon^{m_q+1}}{(1-y\,z_q)^{m_q+1}}\right]\left(\prod_{q=i+1}^{Q-1}\frac{1}{1-z_q}\right)\frac{\prod_{q=1}^{Q}dz_q}{\prod_{q=1}^{Q}z_q-1}\,.\end{aligned}\tag{10}$$

In the last equation, the empty product that appears for $i=0$ is equal to one.

The integrals of z_q $(q=i+1,\,i+2,\ldots,Q-1)$ are calculated in a straightforward manner, since they all exhibit a simple pole at $z_q=1/\left(z_Q\prod_{r=1}^{q-1}z_r\right)$. The successive evaluation of the corresponding residues yields

$$\begin{aligned}I_i&=\frac{1}{(2\pi\jmath)^{i+1}}\oint_{\mathcal{C}_\alpha,\ldots,\mathcal{C}_\beta}\frac{\exp(-\frac{y\,z_Q}{1-y\,z_Q}\,x)}{(1-y\,z_Q)^M\,z_Q}\\&\quad\times\left[\prod_{q=1}^{i}\sum_{m_q=0}^{M-1}\frac{\epsilon^{m_q+1}}{(1-y\,z_q)^{m_q+1}}\right]\frac{dz_Q\prod_{q=1}^{i}dz_q}{z_Q\prod_{q=1}^{i}z_q-1}\,.\end{aligned}\tag{11}$$

We introduce $\pi_j=z_Q\prod_{q=j}^{i}z_q$ and integrate over variable z_1. The only pole resides in $z_1=1/\pi_2$, since $|\pi_1|>1$, and the corresponding integral equals

$$
\begin{aligned}
I_1 &= \frac{1}{2\pi\jmath}\oint_{\mathcal{C}_\alpha}\sum_{m_1=0}^{M-1}\frac{\epsilon^{m_1+1}}{(1-y\,z_1)^{m_1+1}}\,\frac{dz_1}{z_1\,\pi_2-1}\\
&= \frac{1}{\pi_2}\sum_{m_1=0}^{M-1}\frac{\epsilon^{m_1+1}}{(1-\frac{y}{\pi_2})^{m_1+1}}\\
&= \frac{1}{\pi_3}\sum_{m_1=0}^{M-1}\epsilon^{m_1+1}\,\frac{z_2^{m_1}}{(z_2-\frac{y}{\pi_3})^{m_1+1}}\\
&= \sum_{m_1=0}^{M-1}\sum_{l_1=0}^{m_1}\binom{m_1}{l_1}\frac{\epsilon^{m_1+1}\,y^{l_1}}{\pi_3^{l_1+1}}\,\frac{1}{(z_2-\frac{y}{\pi_3})^{l_1+1}}\\
&= \sum_{l_1=0}^{M-1}\sum_{m_1=l_1}^{M-1}\binom{m_1}{l_1}\frac{\epsilon^{m_1+1}\,y^{l_1}}{\pi_3^{l_1+1}}\,\frac{1}{(z_2-\frac{y}{\pi_3})^{l_1+1}}\,.
\end{aligned}
\tag{12}
$$

With respect to z_2, the only pole resides in $z_2 = y/\pi_3$ since $|\pi_2| > 1 > y$. Using Cauchy's integral formula for derivatives, the integral evaluates to

$$
\begin{aligned}
I_2 &= \sum_{l_1=0}^{M-1}\sum_{m_1=l_1}^{M-1}\binom{m_1}{l_1}\frac{\epsilon^{m_1+1}\,y^{l_1}}{\pi_3^{l_1+1}}\\
&\quad\times\frac{1}{2\pi\jmath}\oint_{\mathcal{C}_\alpha}\frac{1}{(z_2-\frac{y}{\pi_3})^{l_1+1}}\sum_{m_2=0}^{M-1}\frac{\epsilon^{m_2+1}}{(1-y\,z_2)^{m_2+1}}\,dz_2\\
&= \sum_{l_1=0}^{M-1}\sum_{m_1=l_1}^{M-1}\binom{m_1}{l_1}\frac{\epsilon^{m_1+1}\,y^{2\,l_1}}{\pi_3^{l_1+1}}\sum_{m_2=0}^{M-1}\binom{m_2+l_1}{m_2}\frac{\epsilon^{m_2+1}}{(1-\frac{y^2}{\pi_3})^{m_2+l_1+1}}\\
&= \sum_{l_1=0}^{M-1}\sum_{m_1=l_1}^{M-1}\binom{m_1}{l_1}\frac{\epsilon^{m_1+1}\,y^{2\,l_1}}{\pi_4^{l_1+1}}\sum_{m_2=0}^{M-1}\binom{m_2+l_1}{m_2}\frac{\epsilon^{m_2+1}\,z_3^{m_2}}{(z_3-\frac{y^2}{\pi_4})^{m_2+l_1+1}}\\
&= \sum_{l_1=0}^{M-1}\sum_{m_1=l_1}^{M-1}\binom{m_1}{l_1}\frac{\epsilon^{m_1+1}\,y^{2\,l_1}}{\pi_4^{l_1+1}\,(z_3-\frac{y^2}{\pi_4})^{l_1+1}}\\
&\quad\times\sum_{m_2=0}^{M-1}\binom{m_2+l_1}{m_2}\epsilon^{m_2+1}\sum_{l_2=0}^{m_2}\binom{m_2}{l_2}\,\epsilon^{m_2+1}\,\frac{(\frac{y^2}{\pi_4})^{l_2}}{(z_3-\frac{y^2}{\pi_4})^{l_2}}\\
&= \epsilon^2\sum_{l_1=0}^{M-1}\sum_{l_2=0}^{M-1}C(l_1,0)\,C(l_2,l_1)\,\frac{y^{2\,l_1+2\,l_2}}{\pi_4^{l_1+l_2+1}}\,\frac{1}{(z_3-\frac{y^2}{\pi_4})^{l_2+l_1+1}}\,,
\end{aligned}
\tag{13}
$$

where parameters $C(u, v)$ are calculated from

$$
C(u,v) = \sum_{m=u}^{M-1}\binom{m}{u}\binom{m+v}{m}\,\epsilon^m\,. \tag{14}
$$

By repeating the process for the remaining z_q we arrive at

$$
I_i = \epsilon^i\sum_{l=0}^{i(M-1)}D_i(l)\,y^{i\,l}\,\frac{1}{2\pi\jmath}\oint_{\mathcal{C}_\beta}\frac{\exp(-\frac{y\,z_Q}{1-y\,z_Q}\,x)}{(1-y\,z_Q)^M\,z_Q}\,\frac{1}{(z_Q-y^i)^{l+1}}\,dz_Q\,, \tag{15}
$$

where we have introduced

$$
D_i(l) = \sum_{l_1+\cdots+l_i=l}C(l_1,0)\,C(l_2,l_1)\,C(l_3,l_1+l_2)\,\ldots\,C(l_i,l_1+\cdots+l_{i-1})\,. \tag{16}
$$

The parameters $D_i(l)$ can be calculated in a recursive manner following

$$
\begin{aligned}
D_i(l) &= \sum_{n=0}^{\min(l,M-1)}D_{i-1}(l-n)\,C(n,l-n)\,,\\
D_0(l) &= \delta(l)\,.
\end{aligned}
\tag{17}
$$

The recursive method is advantageous since it enables the gradual calculation of the parameters. Assuming that the calculation has been performed up to some modulation order, then it is possible to utilize the available parameters and calculate the ones that are required for a higher modulation order. Moreover, if multiple modulation orders are studied simultaneously then it is sufficient to calculate the parameters for the highest order under consideration. The analysis for lower orders is performed in a straight-forward manner using a subset of the available parameters.

The integral in (15) has two poles at $z_Q = 0$ and $z_Q = y^i$. For $z_Q = 0$, we find that

$$
I(0) = -\left(\frac{\epsilon}{y}\right)^i\sum_{l=0}^{i(M-1)}(-1)^l\,D_i(l) = -\left(\frac{\epsilon}{y}\right)^i\,, \tag{18}
$$

since

$$
\sum_{l=0}^{i(M-1)}(-1)^l\,D_i(l) = 1\,. \tag{19}
$$

For $z_Q = y^i$, we utilize [16, Eq. (10)] to evaluate

$$
\begin{aligned}
I(y^i) &= \epsilon^i\sum_{l=0}^{i(M-1)}D_i(l)\,y^{i\,l}\,\frac{1}{l!}\,\frac{d^l}{dz_Q}\left[\frac{\exp(-\frac{y\,z_Q}{1-y\,z_Q}\,x)}{(1-y\,z_Q)^M\,z_Q}\right]\Bigg|_{z_Q=y^i}\\
&= \left(\frac{\epsilon}{y}\right)^i\frac{\exp(-\frac{y^{i+1}}{1-y^{i+1}}\,x)}{(1-y^{i+1})^M}\sum_{k=0}^{i(M-1)}d_{k,i}(y)\,L_k^{M-1}\left(\frac{x}{1-y^{i+1}}\right)\,,
\end{aligned}
\tag{20}
$$

where

$$
d_{k,i}(y) = \left(\frac{-y^{i+1}}{1-y^{i+1}}\right)^k\sum_{l=k}^{i(M-1)}(-1)^l\,D_i(l)\,. \tag{21}
$$

By combining the results for $z_Q = 0$ and $z_Q = y^i$, I_i becomes

$$
I_i = \left(\frac{\epsilon}{y}\right)^i\left[\frac{\exp(-\frac{y^{i+1}}{1-y^{i+1}}\,x)}{(1-y^{i+1})^M}\sum_{k=0}^{i(M-1)}d_{k,i}(y)\,L_k^{M-1}\left(\frac{x}{1-y^{i+1}}\right)-1\right] \tag{22}
$$

and $P_{c,s}$ is calculated after combining (22) and (7) as

$$
\begin{aligned}
P_{c,s} &= \epsilon^M\sum_{i=0}^{Q-1}\binom{Q-1}{i}(-1)^i\,\frac{\exp(-\frac{1-y^i}{1-y^{i+1}}\,\epsilon\,\mu_s)}{(1-y^{i+1})^M}\\
&\qquad\times\sum_{k=0}^{i(M-1)}d_{k,i}(y)\,L_k^{M-1}\left(\frac{x}{1-y^{i+1}}\right)\,.
\end{aligned}
\tag{23}
$$

Finally, the symbol-error probability $P_{e,s} = 1 - P_{c,s}$ is given by

$$
\begin{aligned}
P_{e,s} &= \epsilon^M\sum_{i=1}^{Q-1}\binom{Q-1}{i}(-1)^{i+1}\,\frac{\exp(-\frac{1-y^i}{1-y^{i+1}}\,\epsilon\,\mu_s)}{(1-y^{i+1})^M}\\
&\qquad\times\sum_{k=0}^{i(M-1)}d_{k,i}(y)\,L_k^{M-1}\left(\frac{x}{1-y^{i+1}}\right)
\end{aligned}
\tag{24}
$$

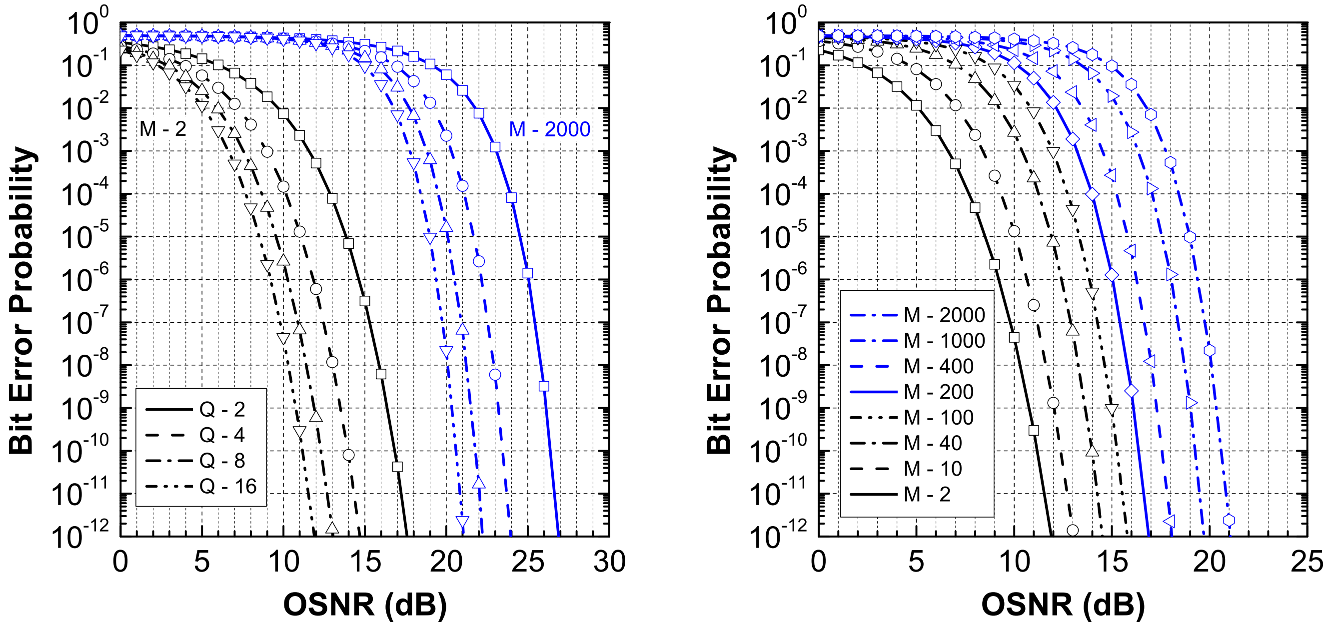

(a) $M = 2, 2000$ and $Q = 2, 4, 8, 16$ (b) $M = 2, \ldots, 2000$ and $Q = 16$.

Fig. 1. BEP for a preamplified PPM receiver. Plot lines correspond to finite summation and markers correspond to infinite summation based on (3).

and the BEP $P_{e,b}$ becomes [10]

$$P_{e,b} = \frac{Q}{2\,(Q-1)}\,P_{e,s}\,, \tag{25}$$

respectively, which require the summation over a finite number of terms. Moreover, parameters $d_{k,i}(y)$ do not depend on the signal photons and it is possible to pre-calculate, store and reuse them in order to evaluate the BEP for the desired range of signal energies. The finite summation over signal-independent terms also enables the efficient evaluation of the BEP in applications with a varying number of received signal photons, as is the case in atmospheric transmission systems where scintillations and pointing errors introduce non-constant path losses. Note that in these applications, the calculation of the infinite sum of (3) proves even more problematic since each of the signal-dependent terms is replaced by expressions that involve the Meijer G-function, as we detail in Sections 3 and 4.

2.2. Validation of results

To validate the results that are obtained from (25), we consider a pre-amplified system, where an optical amplifier is used before the direct detection photodiode to improve its sensitivity. The amplifier gain is G and the noise photons that are generated per noise mode equal $\lambda = n_{sp}\,(G-1)$, where n_{sp} is the spontaneous emission factor. The amplifier output is filtered by an optical filter with a bandwidth equal to B_o and as a result the noise modes equal $M = p\,B_o\,T_s$, where T_s is the PPM slot duration and p are the polarization modes that enter the receiver (typically two). The amplified signal photons are equal to $\mu_s = G\,\mu_b\,\log_2(Q)$, where μ_b is the number of photons per received bit at the amplifier input. Next, we present our analytical results with respect to the signal to noise energy ratio at the amplifier input $OSNR = \mu_b/n_{sp}$, which practically coincides with the OSNR at the amplifier output for high optical gains.

Fig. 1 shows the bit-error probability for a pre-amplified receiver with $G = 100$ and $n_{sp} = 1$. The noise modes range between $M = 2 - 2000$ and PPM orders are equal to $Q = 2, 4, 8, 16$. The results serve to verify the validity of our approach, and no difference is observed between finite and infinite summation for BEPs as low as 10^{-12}, irrespectively of the noise modes and modulation order. As expected, a significant OSNR gain is observed as increasing modulation orders, with $Q = 4$ providing a 3 dB benefit while requiring the same bandwidth compared to $Q = 2$, thus justifying its utilization in recent transmission experiments. An increase in the noise modes, on the other hand, always proves detrimental and a penalty of approximately 1 dB is introduced when the noise modes are doubled.

3. Q-PPM ABEP performance over fading

We consider an optical wireless link where the optical signal propagates through the atmosphere, and the atmospheric scintillations introduce a random fluctuation h_a on the number of the received signal photons. The instantaneous value of the number of photons at the receiver input equals $\mu_s\,h_a$ and the corresponding conditional BEP on h_a is calculated from (25) as

$$P_{e,b} = \frac{Q\,\epsilon^M}{2\,(Q-1)} \sum_{i=1}^{Q-1} \binom{Q-1}{i} (-1)^{i+1} \frac{\exp\left(-\frac{1-y^i}{1-y^{i+1}}\,\epsilon\,\mu_s\,h_a\right)}{(1-y^{i+1})^M} \times \sum_{k=0}^{i(M-1)} d_{k,i}(y)\,L_k^{M-1}\left(\frac{x\,h_a}{1-y^{i+1}}\right). \tag{26}$$

The ABEP is obtained by integrating (26) over the probability density function (pdf) of h_a. For the random fluctuations we consider the generalized Malaga-$\mathcal{M}$ model, which quantifies the effect of weak, moderate and strong scintillations in a unified manner.

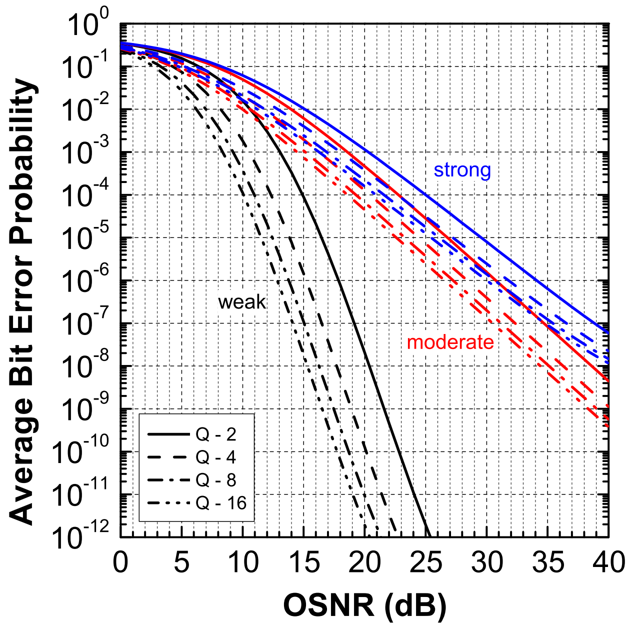

(a) Noise modes are equal to $M = 2$.

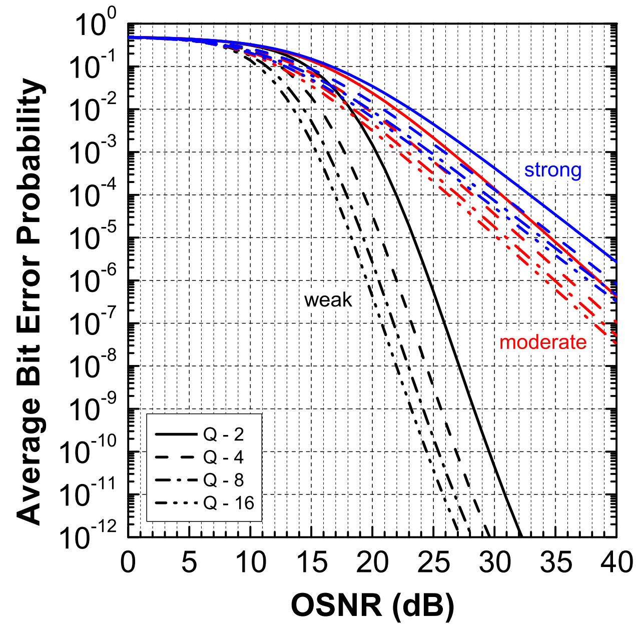

(b) Noise modes are equal to $M = 200$.

Fig. 2. ABEP of PPM modulation for weak, moderate and strong Malaga-$\mathcal{M}$ fading.

3.1. ABEP over normalized Malaga-$\mathcal{M}$ fading

The pdf of normalized Malaga-$\mathcal{M}$ distributed random variables (RVs) is [23]

$$
\begin{aligned}
f_{h_a}(h_a) &= \frac{1}{h_a} \sum_{j=1}^{\beta} b_j \, G_{0,2}^{2,0}\left(\delta\, h_a \,\middle|\, \begin{matrix} - \\ \alpha, j \end{matrix} \right), \\
\delta &= \frac{\alpha\,\beta\,(\gamma + \Omega')}{\gamma\,\beta + \Omega'}, \\
b_j &= \frac{A}{2}\, a_j \left(\frac{\alpha\,\beta}{\gamma\,\beta + \Omega'} \right)^{-\frac{a+j}{2}},
\end{aligned} \tag{27}
$$

where $G_{p,q}^{m,n}(\cdot)$ is the Meijer G-function [20, eq. (9.301)] and the Malaga-$\mathcal{M}$ model parameters $\alpha, \beta, \gamma, \Omega'$ are described in detail in the literature [23], along with the calculation of A, a_j.

The ABEP calculation requires the evaluation of the integral

$$
\begin{aligned}
I &= \int_0^{\infty} \exp\left(-\frac{1 - y^i}{1 - y^{i+1}}\, \epsilon\, \mu_s\, h_a \right) \\
&\quad \times L_k^{M-1}\left(\frac{x\, h_a}{1 - y^{i+1}} \right) G_{0,2}^{2,0}\left(\delta\, h_a \,\middle|\, \begin{matrix} - \\ \alpha, j \end{matrix} \right) \frac{dh_a}{h_a} \\
&= \sum_{n=0}^{k} \binom{k+M-1}{n+M-1} \left(\frac{-x}{1 - y^{i+1}} \right)^n \\
&\times \frac{1}{n!} \int_0^{\infty} h_a^{n-1} \exp\left(-\frac{1 - y^i}{1 - y^{i+1}}\, \epsilon\, \mu_s\, h_a \right) G_{0,2}^{2,0}\left(\delta\, h_a \,\middle|\, \begin{matrix} - \\ \alpha, j \end{matrix} \right) dh_a \\
&= \sum_{n=0}^{k} \binom{k+M-1}{n+M-1} \left(\frac{\epsilon}{y\,(1 - y^i)} \right)^n \\
&\quad \times \frac{1}{n!}\, G_{1,2}^{2,1}\left(\frac{\delta\,(1 - y^{i+1})}{\epsilon\, \mu_s\,(1 - y^i)} \,\middle|\, \begin{matrix} 1-n \\ \alpha, j \end{matrix} \right),
\end{aligned} \tag{28}
$$

Table 1
Malaga-$\mathcal{M}$ Distribution Parameter Values.

Parameter	Irradiance Fluctuations		
	Weak	Moderate	Strong
α	50	2.55	2.281
β	14	22	33
γ	0.006	0.016	0.135
Ω'	1.099	1.751	2.04

where we expanded the Laguerre polynomials following [20, eq. (8.970/1)] and used [20, eq. (7.813)] for the integral of the Meijer G-function. After sum term re-arrangements, the final expression for the ABEP becomes

$$
\begin{aligned}
\overline{P}_{e,b} &= \frac{Q\,\epsilon^M}{2\,(Q-1)} \sum_{i=1}^{Q-1} \binom{Q-1}{i} (-1)^{i+1} \frac{1}{(1 - y^{i+1})^M} \\
&\quad \times \sum_{n=0}^{i(M-1)} \sum_{k=n}^{i(M-1)} \binom{k+M-1}{n+M-1} d_{k,i}(y) \left(\frac{\epsilon}{y\,(1 - y^i)} \right)^n \\
&\quad \times \frac{1}{n!} \sum_{j=1}^{\beta} b_j\, G_{1,2}^{2,1}\left(\frac{\delta\,(1 - y^{i+1})}{\epsilon\, \mu_s\,(1 - y^i)} \,\middle|\, \begin{matrix} 1-n \\ \alpha, j \end{matrix} \right).
\end{aligned} \tag{29}
$$

Eq. (29) is plotted in Fig. 2 for weak, moderate and strong Malaga-$\mathcal{M}$ fading. The distribution parameters are taken from [23] and are summarized in Table 1. The results show that an increase in the modulation order provides a very significant benefit in weak fading. In high OSNRs, where the ABEP attains a constant slope, 4-PPM reduces the ABEP by two orders of magnitude in comparison to 2-PPM, and 16-PPM further reduces the ABEP by the same amount. The improvement is less significant in moderate and strong fading, where the ABEP is decreased by approximately a factor of 10 in 16-PPM. These observations hold for both noise mode values under consideration ($M = 2, 200$), although higher OSNRs are required for a given ABEP target at increased noise modes, as expected.

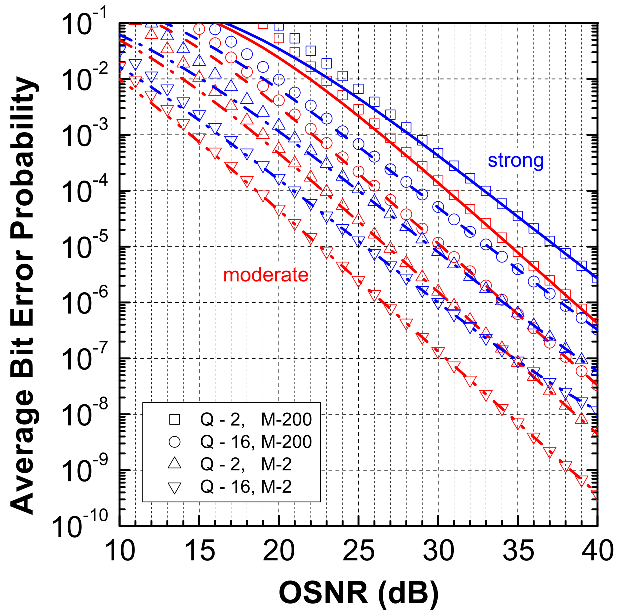

Fig. 3. Exact and asymptotic ABEP of PPM modulation for moderate and strong Malaga-$\mathcal{M}$ fading.

3.2. Asymptotic ABEP approximation

The evaluation of the ABEP at high OSNRs can be facilitated by expanding the Meijer G-function in Eq. (29) as the sum of ${}_1F_1(\cdot)$ hypergeometric functions. We utilize [20, eq. (9.303)] to obtain

$$G_{1,2}^{2,1}\left(z \,\middle|\, \begin{matrix} 1-n \\ \alpha, j \end{matrix}\right) = z^j \,\Gamma(j+n)\,\Gamma(\alpha-j)\,{}_1F_1\,(j+n;\ 1+j-\alpha;\ z) + z^\alpha\,\Gamma(\alpha+n)\,\Gamma(j-\alpha)\,{}_1F_1\,(\alpha+n;\ 1+\alpha-j;\ z)\,, \tag{30}$$

where $\Gamma(\cdot)$ is the Gamma function. For sufficiently high OSNRs, the argument of the Meijer-G function attains values near zero, and we approximate the hypergeometric function by keeping the leading term. This yields the following approximation of the Meijer-G function

$$G_{1,2}^{2,1}\left(z \,\middle|\, \begin{matrix} 1-n \\ \alpha, j \end{matrix}\right) \approxeq z^\alpha\,\Gamma(\alpha+n)\,\Gamma(j-\alpha) + z^j\,\Gamma(j+n)\,\Gamma(\alpha-j)\,. \tag{31}$$

The exact results of Eq. (29) are compared with the approximation in Fig. 3, and the validity of the approximation is verified from the figure, especially at high OSNRs. It should be noted, however, that the approximation is not valid in weak fading, mainly because the Malaga-$\mathcal{M}$ parameter δ attains an increased value and higher OSNRs are required to achieve asymptotic behavior. Due to weak fading, this lead to ABEPs lower than 10^{-12}, which are beyond the scope of this work.

3.3. ABEP over $\gamma-\gamma$ and negative exponential fading

Analytical results can also be obtained for $\gamma-\gamma$ fading, since the corresponding distribution has a functional form that resembles the Malaga-$\mathcal{M}$ one. In the $\gamma-\gamma$ model, the channel fluctuations h_a are distributed as [24]

Table 2
$\gamma-\gamma$ Distribution Parameter Values.

Parameter	l-100 m	l-275 m	l-325 m	l-1000 m
α	16.5347	4.62457	4.22772	5.50966
β	14.9057	2.8674	2.3177	1.1138

$$f_{h_a}(h_a) = \frac{1}{\Gamma(\alpha)\,\Gamma(\beta)\,h_a}\,G_{0,2}^{2,0}\left(\alpha\,\beta\,h_a \,\middle|\, \begin{matrix} - \\ \alpha, \beta \end{matrix}\right)\,. \tag{32}$$

The distribution parameters α and β are calculated from [25, eq. (5.15, 9.41, 9.46, 9.138)]. Following a similar analysis as in Section 3.1, the ABEP evaluates to

$$\begin{aligned}\overline{P}_{e,b} = {} & \frac{Q\,\epsilon^M}{2\,(Q-1)\,\Gamma(\alpha)\,\Gamma(\beta)}\sum_{i=1}^{Q-1}\binom{Q-1}{i}\frac{(-1)^{i+1}}{(1-y^{i+1})^M} \\ & \times \sum_{n=0}^{i(M-1)}\sum_{k=n}^{i(M-1)}\binom{k+M-1}{n+M-1}\,d_{k,i}(y)\left(\frac{\epsilon}{y\,(1-y^i)}\right)^n \\ & \times \frac{1}{n!}\,G_{1,2}^{2,1}\left(\frac{\alpha\,\beta\,(1-y^{i+1})}{\epsilon\,\mu_s\,(1-y^i)} \,\middle|\, \begin{matrix} 1-n \\ \alpha, \beta \end{matrix}\right)\,. \end{aligned} \tag{33}$$

The $\gamma-\gamma$ and Malaga-$\mathcal{M}$ ABEPs are compared in Fig. 4 for 16-PPM and $M=200$ noise modes. The $\gamma-\gamma$ parameters are summarized in Table 2 and are evaluated for a wavelength of 1550 nm and for a structure constant equal to $C_n^2 = 4.58\cdot 10^{-13}$ m$^{-2/3}$. Comparable results are obtained between the two distributions when the transmission length in the $\gamma-\gamma$ model is equal to 100, 275 and 325 m. In addition, a longer transmission length of 1000 m is included in the figure to demonstrate the applicability of our analytical relations in severe fading. In this scenario, the $\gamma-\gamma$ ABEP performance resembles the one of a negative exponential fading model, where h_a is distributed as [25]

$$f_{h_a}(h_a) = e^{-h_a} = G_{0,1}^{1,0}\left(h_a \,\middle|\, \begin{matrix} - \\ 0 \end{matrix}\right) \tag{34}$$

and the corresponding ABEP equals

$$\begin{aligned}\overline{P}_{e,b} = {} & \frac{Q\,\epsilon^M}{2\,(Q-1)}\sum_{i=1}^{Q-1}\binom{Q-1}{i}(-1)^{i+1}\frac{1}{(1-y^{i+1})^M} \\ & \times \sum_{n=0}^{i(M-1)}\sum_{k=n}^{i(M-1)}\binom{k+M-1}{n+M-1}\,d_{k,i}(y)\left(\frac{\epsilon}{y\,(1-y^i)}\right)^n \\ & \times \frac{1}{n!}\,G_{1,1}^{1,1}\left(\frac{1-y^{i+1}}{\epsilon\,\mu_s\,(1-y^i)} \,\middle|\, \begin{matrix} 1-n \\ 1 \end{matrix}\right)\,. \end{aligned} \tag{35}$$

3.4. ABEP of multi-branch receivers over normalized Malaga-$\mathcal{M}$ fading

We also consider a multiple receiver architecture, where L preamplified branches are utilized in order to partially mitigate the adverse impact of irradiance fluctuations. In this arrangement, the received photon counts are added in an equal-gain combiner (EGC) prior to PPM demodulation. This type of combiner is relatively simple to implement, since it does not require estimations for the channel state or the signal energy level, while at the same time it achieves comparable results with more complex multi-branch architectures [26].

Assuming that the amplifiers have identical gains and spontaneous emission factors, independent and identically distributed

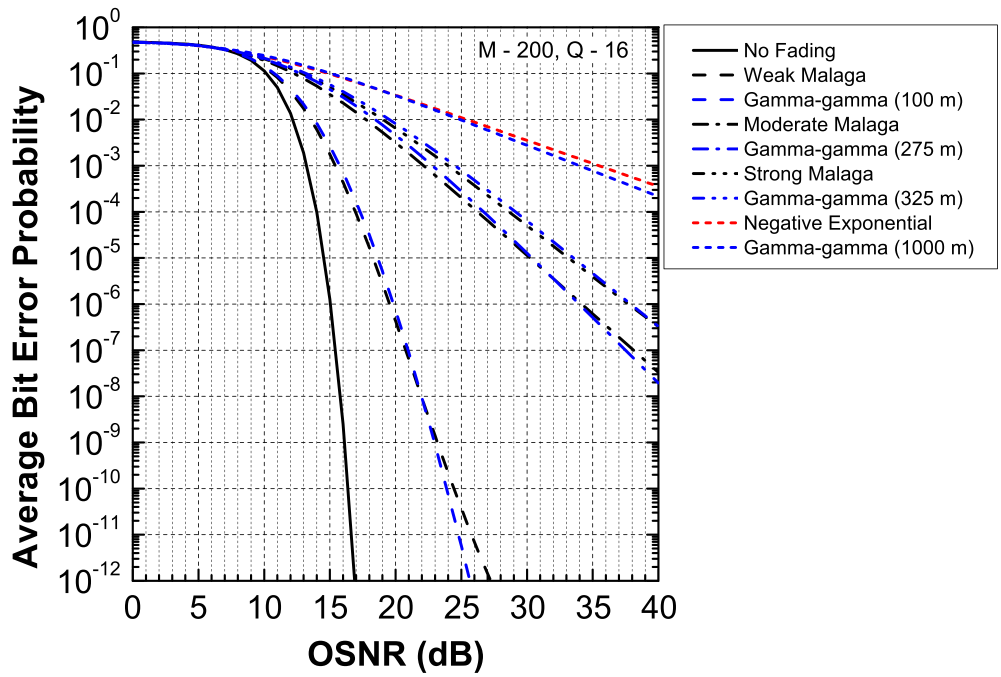

Fig. 4. ABEP in Malaga-$\mathcal{M}$, $\gamma - \gamma$ and negative exponential fading for 16-PPM and $M = 200$ noise modes.

RVs for the noise signals are generated, and the EGC output follows a Laguerre distribution with an increased number of noise modes $N = LM$ [18]. Moreover, the total number of signal photons at the EGC output equals $\mu_s \sum_{\ell=1}^{L} h_{a,\ell}/L$, where $h_{a,\ell}$ denotes the ℓth channel response. For the rest of our analysis, it is assumed that the lateral separation of the receiver branches is adequate and the received signals $h_{a,\ell}\,\mu_s$ are distributed as independent Malaga-$\mathcal{M}$ RVs.

Similarly to the single-branch analysis, the conditional BEP is calculated as

$$
\begin{aligned}
P_{e,b} &= \frac{Q\,\epsilon^N}{2\,(Q-1)} \sum_{i=1}^{Q-1} \binom{Q-1}{i} (-1)^{i+1} \frac{\exp\left(-\frac{1-y^i}{1-y^{i+1}} \frac{\epsilon\,\mu_s}{L} \sum_{\ell=1}^{L} h_{a,\ell}\right)}{(1-y^{i+1})^N} \\
&\quad \times \sum_{k=0}^{i(N-1)} d_{k,i}(y)\, L_k^{N-1}\left(\frac{x}{L\,(1-y^{i+1})} \sum_{\ell=1}^{L} h_{a,\ell}\right), \\
&= \frac{Q\,\epsilon^N}{2\,(Q-1)} \sum_{i=1}^{Q-1} \binom{Q-1}{i} (-1)^{i+1} \frac{1}{(1-y^{i+1})^N} \\
&\quad \times \sum_{k=0}^{i(N-1)} d_{k,i}(y) \sum_{n=0}^{k} \binom{k+N-1}{n+N-1} \left[\frac{-x}{L\,(1-y^{i+1})}\right]^n \\
&\quad \times \sum_{n_1+\cdots+n_L=n} \prod_{\ell=1}^{L} \frac{h_{a,\ell}^{n_\ell}}{n_\ell!} \exp\left(-\frac{1-y^i}{1-y^{i+1}} \frac{\epsilon\,\mu_s}{L} h_{a,\ell}\right).
\end{aligned} \tag{36}
$$

Using (28), the ABEP of the EGC is evaluated as

$$
\begin{aligned}
\overline{P}_{e,b} &= \frac{Q\,\epsilon^N}{2\,(Q-1)} \sum_{i=1}^{Q-1} \binom{Q-1}{i} (-1)^{i+1} \frac{1}{(1-y^{i+1})^N} \\
&\quad \times \sum_{k=0}^{i(N-1)} d_{k,i}(y) \sum_{n=0}^{k} \binom{k+N-1}{n+N-1} \left[\frac{\epsilon}{y\,(1-y^i)}\right]^n \\
&\quad \times \sum_{n_1+\cdots+n_L=n} \prod_{\ell=1}^{L} \frac{1}{n_\ell!} \sum_{j=1}^{\beta} b_j\, G_{1,2}^{2,1}\left(\frac{L\,\delta\,(1-y^{i+1})}{\epsilon\,\mu_s\,(1-y^i)} \,\middle|\, \begin{matrix} 1-n_\ell \\ \alpha, j \end{matrix}\right),
\end{aligned} \tag{37}
$$

and we introduce the definitions of the extended binomial coefficients

$$
\begin{aligned}
w(s) &= \frac{1}{s!} \sum_{j=1}^{\beta} b_j\, G_{1,2}^{2,1}\left(\frac{L\,\delta\,(1-y^{i+1})}{\epsilon\,\mu_s\,(1-y^i)} \,\middle|\, \begin{matrix} 1-s \\ \alpha, j \end{matrix}\right), \\
\binom{L}{n}_w &= \sum_{n_1+\cdots+n_L=n} \prod_{\ell=1}^{L} w(n_\ell),
\end{aligned} \tag{38}
$$

to arrive at

$$
\begin{aligned}
\overline{P}_{e,b} &= \frac{Q\,\epsilon^N}{2\,(Q-1)} \sum_{i=1}^{Q-1} \binom{Q-1}{i} (-1)^{i+1} \frac{1}{(1-y^{i+1})^N} \\
&\quad \times \sum_{n=0}^{i(N-1)} \sum_{k=n}^{i(N-1)} \binom{k+N-1}{n+N-1} d_{k,i}(y) \left[\frac{\epsilon}{y\,(1-y^i)}\right]^n \binom{L}{n}_w .
\end{aligned} \tag{39}
$$

The coefficients $\binom{L}{n}_w$ can be efficiently calculated using the recursion formula [27, Eq. (4)]

$$
\begin{aligned}
\binom{L}{n}_w &= \sum_{s=0}^{n} w(s) \binom{L-1}{n-s}_w , \\
\binom{0}{n}_w &= \delta_n
\end{aligned} \tag{40}
$$

which re-uses the previously calculated values of the Meijer G-function.

The ABEP performance of the EGC receiver is presented in Fig. 5 for 16-PPM and up to $L = 10$ branches. In weak fading, the utilization of additional branches proves detrimental at low OSNRs due to the excess noise that is generated by the amplifiers, and this effect becomes worse for an increased number of noise modes ($M = 200$). The performance of the multi-branch receiver improves at higher OSNRs and a gain of a couple dB is observed when the second receiver is introduced. A further increase in the number of the branches above two provides a limited improvement which may not justify the associated implementation cost, complexity and energy consumption of such a multi-branch in

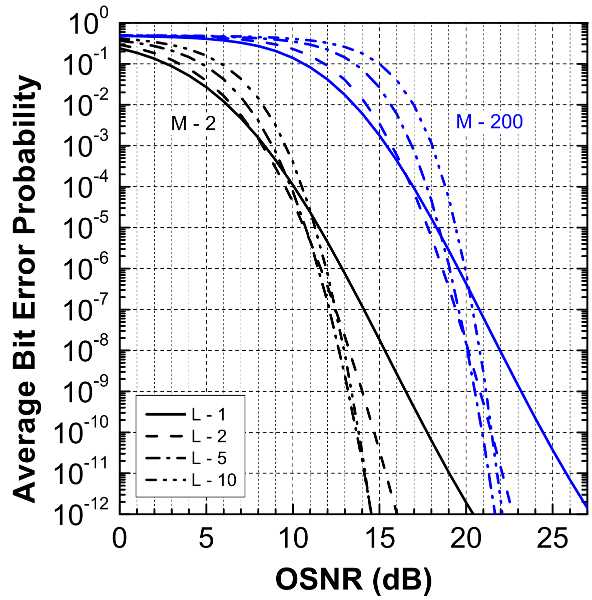

(a) Weak Malaga-$\mathcal{M}$ fading.

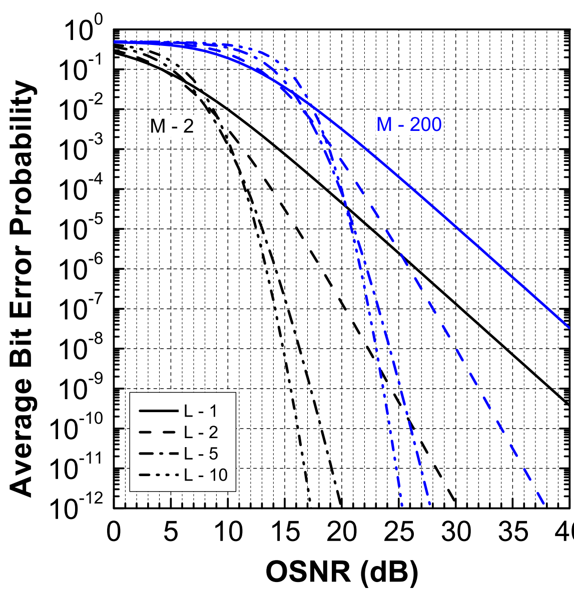

(b) Moderate Malaga-$\mathcal{M}$ fading.

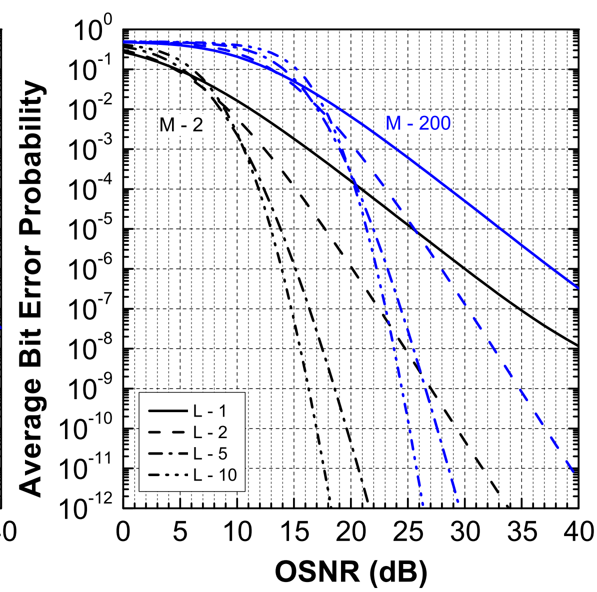

(c) Strong Malaga-$\mathcal{M}$ fading.

Fig. 5. ABEP for EGC reception of 16-PPM in weak, moderate and strong Malaga-$\mathcal{M}$ fading.

weak fading, unless mandated by additional impairments such imperfect tracking and acquisition, beam wander, or a requirement for increased reliability [5,6]. The utilization of five and ten receivers is more appealing in moderate and strong fading. In these application scenarios, the diversity gain outweighs the amplification noise penalty and significant overall gains are observed for both a reduced ($M = 2$) and an increased ($M = 200$) number of noise modes.

4. Q-PPM ABEP performance over fading and pointing errors

The introduction of pointing errors modifies the channel response to $h = h_a h_p$, where h_a and h_p are RVs that model the impact of fading and pointing errors, respectively. Pointing errors introduced by misalignments are modeled as Gaussian RVs [28]. It has been previously shown that the distribution of h_p can be approximated by [29]

$$f_{h_p}(h_p) = \frac{\phi^2}{A^{\phi^2}} h_p^{\phi^2-1}, \; 0 \le h_p \le A. \tag{41}$$

The distribution parameters ϕ and A are calculated from the receiver aperture radius a, the beam-width at the receiver w_z and the misalignment mean values μ_x and μ_y and variances σ_x and σ_y [29]. Given (27) and (41), the channel response h is distributed as [30]

$$f_h(h) = \frac{\phi^2}{h} \sum_{j=1}^{\beta} b_j G_{1,3}^{3,0}\left(\frac{\delta h}{A} \middle| \begin{matrix} \phi^2 + 1 \\ \phi^2, \alpha, j \end{matrix} \right). \tag{42}$$

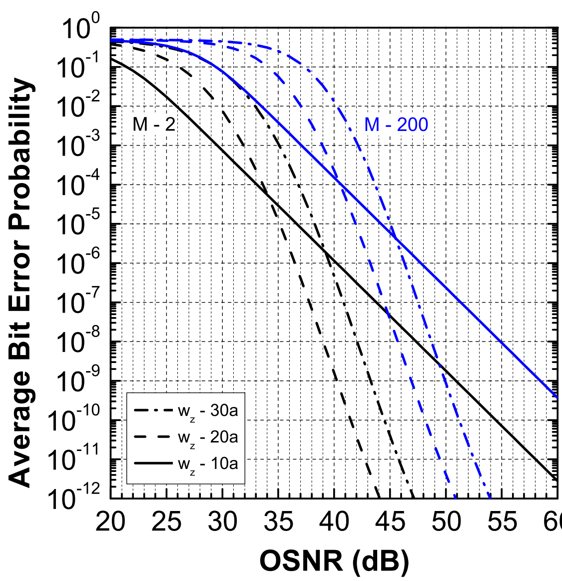

(a) Weak Malaga-$\mathcal{M}$ fading.

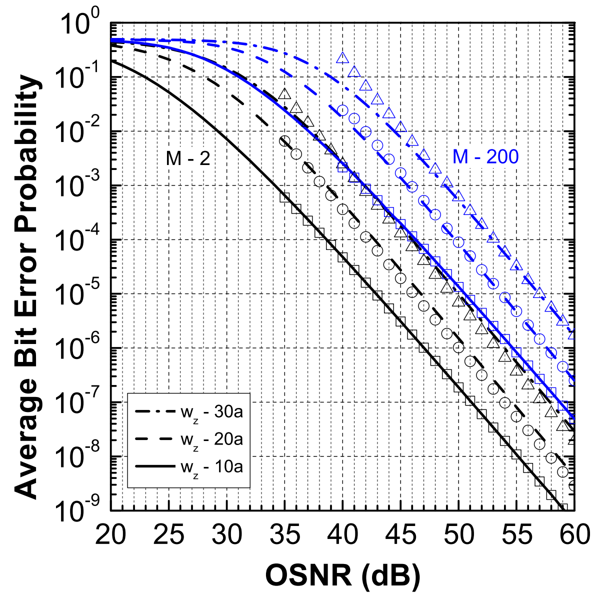

(b) Moderate Malaga-$\mathcal{M}$ fading.

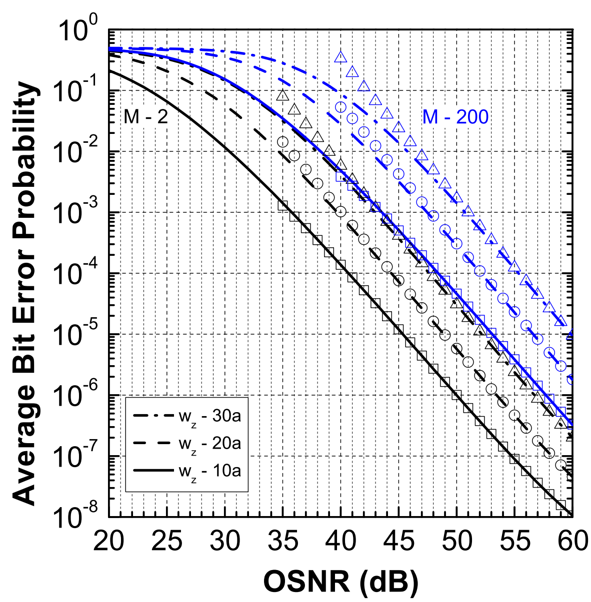

(c) Strong Malaga-$\mathcal{M}$ fading.

Fig. 6. ABEP for 16-PPM in weak, moderate and strong Malaga-$\mathcal{M}$ fading with pointing errors. Markers correspond to the asymptotic approximation.

The conditional BEP is identical to (26) and using [20, eq. (7.813), (8.970/1)]

$$\begin{aligned} I &= \int_0^\infty \exp\left(-\frac{1-y^i}{1-y^{i+1}}\,\epsilon\,\mu_s\,h\right) \\ &\quad \times L_k^{M-1}\left(\frac{x\,h}{1-y^{i+1}}\right)\frac{1}{h}\,G_{1,3}^{3,0}\left(\frac{\delta\,h}{A}\,\middle|\,\begin{matrix}\phi^2+1\\ \phi^2,\alpha,j\end{matrix}\right)dh \\ &= \sum_{n=0}^{k}\binom{k+M-1}{n+M-1}\left(\frac{\epsilon}{y\,(1-y^i)}\right)^n \\ &\quad \times \frac{1}{n!}\,G_{2,3}^{3,1}\left(\frac{\delta\,(1-y^{i+1})}{A\,\epsilon\,\mu_s\,(1-y^i)}\,\middle|\,\begin{matrix}1-n,\phi^2+1\\ \phi^2,\alpha,j\end{matrix}\right) \end{aligned} \tag{43}$$

and the ABEP is given by

$$\begin{aligned} \overline{P}_{e,b} &= \frac{Q\,\epsilon^M}{2\,(Q-1)}\sum_{i=1}^{Q-1}\binom{Q-1}{i}(-1)^{i+1}\frac{1}{(1-y^{i+1})^M} \\ &\quad \times \sum_{n=0}^{i(M-1)}\sum_{k=n}^{i(M-1)}\binom{k+M-1}{n+M-1}d_{k,i}(y)\left(\frac{\epsilon}{y\,(1-y^i)}\right)^n \\ &\quad \times \frac{\phi^2}{n!}\sum_{j=1}^{\beta}b_j G_{2,3}^{3,1}\left(\frac{\delta\,(1-y^{i+1})}{A\,\epsilon\,\mu_s\,(1-y^i)}\,\middle|\,\begin{matrix}1-n,\phi^2+1\\ \phi^2,\alpha,j\end{matrix}\right). \end{aligned} \tag{44}$$

The ABEP performance is presented in Fig. 6 for a 16-PPM system and for pointing error parameters that are summarized in Table 3. The table values correspond to a zero boresight error $\mu_x = \mu_y =$

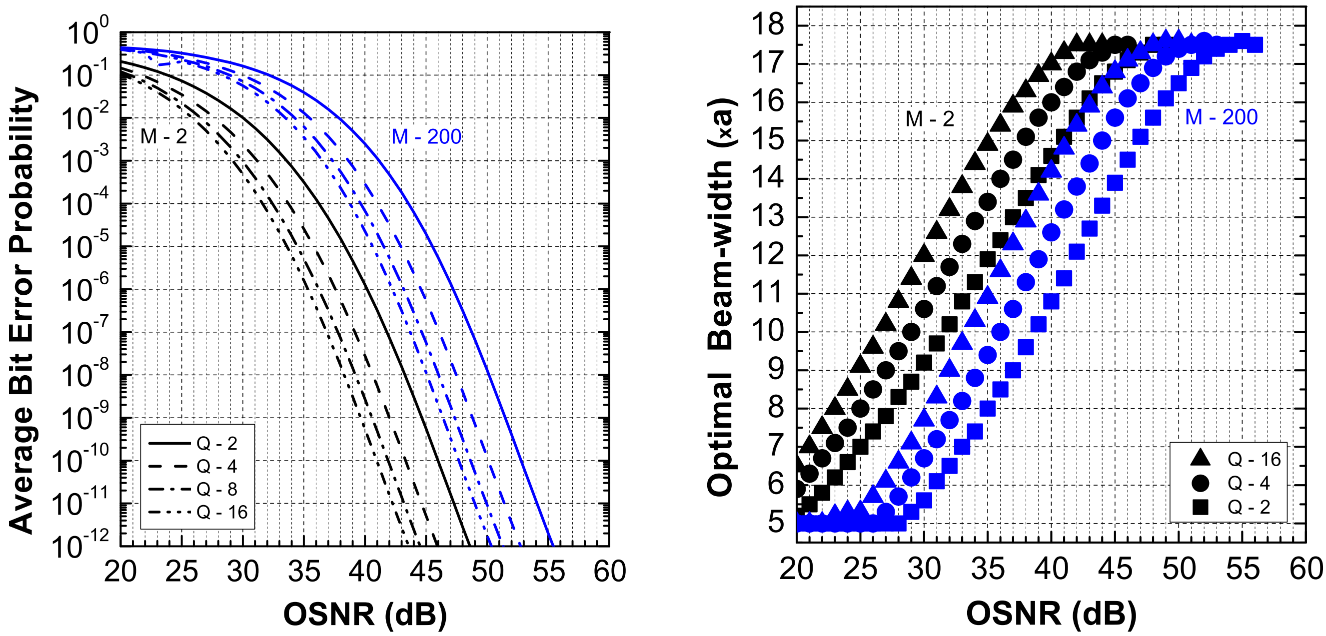

(a) Optimal ABEP. (b) Optimal beam-width.

Fig. 7. Optimal ABEP and beam-width in weak Malaga-$\mathcal{M}$ fading with pointing errors.

Table 3
Pointing Errors Parameter Values.

Parameter	Values		
w_z/a	10	20	30
A	0.020	0.005	0.002
ϕ^2	2.807	11.14	25.029

0 and equal jitters $\sigma_x = \sigma_y = 3\,a$. The figure also presents results that are obtained using the asymptotic expression

$$G_{2,3}^{3,1}\left(z \,\middle|\, \begin{matrix} 1-n, \phi^2+1 \\ \phi^2, \alpha, j \end{matrix}\right) \approx z^{\phi^2}\,\Gamma(\phi^2+n)\,\Gamma(\alpha-\phi^2)\,\Gamma(j-\phi^2) + z^j\,\frac{\Gamma(j+n)\,\Gamma(\alpha-j)}{\phi^2-j} + z^{\alpha}\,\frac{\Gamma(\alpha+n)\,\Gamma(j-\alpha)}{\phi^2-\alpha}, \tag{45}$$

which is derived from [20, eq. (9.303)] and after keeping the first term of the appearing hypergeometric functions.

The results show that the ABEP performance is determined by the relative strength of the fading and pointing errors. In weak fading, a narrow beam-with equal to $w_z = 10\,a$ is preferable at lower OSNRs, but the beam must be expanded to $w_z = 20\,a$ at higher OSNRs. Expanding the beam introduces a power penalty due to the increase in the static losses A, but this is compensated by the fact that a broader beam is more resilient to random misalignments, and a net gain is observed. This approach, however, is not applicable in moderate and strong fading, where the impact of fading is far more detrimental than that of pointing errors. In this regime, the results show that the utilization of a broader beam worsens the ABEP and that the narrowest beam-width should be utilized.

The presented analytical relations are further investigated for the optimization of the beam-width and the ABEP in weak fading. To this end, we repeatedly calculate (44) to locate the beam-width that minimizes the ABEP. The optimal beam-width is determined with an accuracy of $\delta w_z = \pm 0.1\,a$ and the results of the optimization process are presented in Fig. 7. The results show that the optimal beam-width increases with the OSNR, as expected from the previous figure, and that both the modulation order and the noise modes affect its values. Higher modulation orders allow for the utilization of broader beams, given that they provide a better receiver sensitivity. On the other hand, an increase in the noise modes worsens the receiver performance at any given OSNR level and therefore the optimal beam-width is reduced.

5. Conclusion

We have derived analytical relations for the BEP performance of optically amplified PPM receivers using the photon counting Laguerre noise distribution. The proposed relations are exact, not limited to the binary modulation format, require a finite summation, and involve constants that can be stored and re-used for the more efficient calculation of the BEP. This approach also enables the efficient calculation of the ABEP in scenarios where the received signal energy fluctuates due to fading or pointing errors, since the aforementioned constants only depend on the amplifier noise. We have shown that ABEP calculation in scenarios with fading and pointing error requires similar finite sums. We have presented results on weak, moderate and strong fading conditions considering widely accepted distributions and demonstrated the beneficial effects of spatial diversity in moderate and strong fading. Finally, we have presented results on the combined impact of fading and pointing errors, verifying that the beam-width at the receiver plays a key role, especially in weak fading where the two impairments assume comparable strengths.

CRediT authorship contribution statement

Konstantinos Yiannopoulos: Concept, Design, Analysis, Writing – review & editing. **Nikos C. Sagias:** Concept, Design, Analysis, Writing – review & editing. **Anthony C. Boucouvalas:** Concept, Design, Analysis, Writing – review & editing.

Declaration of competing interest

The authors declare that they have no known competing financial interests or personal relationships that could have appeared to influence the work reported in this paper.

References

[1] X. Zhu, J. Kahn, Free-space optical communication through atmospheric turbulence channels, IEEE Trans. Commun. 50 (8) (2002) 1293–1300, http://dx.doi.org/10.1109/TCOMM.2002.800829.

[2] V.W.S. Chan, Free-space optical communications, J. Lightwave Technol. 24 (12) (2006) 4750–4762, http://dx.doi.org/10.1109/JLT.2006.885252.

[3] D.K. Borah, A.C. Boucouvalas, C.C. Davis, S. Hranilovic, K. Yiannopoulos, A review of communication oriented optical wireless systems, EURASIP J. Wireless Commun. Networking (91) (2012) 1–28, http://dx.doi.org/10.1186/1687-1499-2012-91.

[4] M.A. Khalighi, M. Uysal, Survey on free space optical communication: A communication theory perspective, IEEE Commun. Surv. Tutor. 16 (4) (2014) 2231–2258, http://dx.doi.org/10.1109/COMST.2014.2329501.

[5] D.M. Boroson, J.J. Scozzafava, D.V. Murphy, B.S. Robinson, M.I.T. Lincoln, The lunar laser communications demonstration (LLCD), in: 2009 Third IEEE International Conference on Space Mission Challenges for Information Technology, 2009, pp. 23–28, http://dx.doi.org/10.1109/SMC-IT.2009.57.

[6] F.I. Khatri, B.S. Robinson, M.D. Semprucci, D.M. Boroson, Lunar laser communication demonstration operations architecture, Acta Astronaut. 111 (2015) 77–83, http://dx.doi.org/10.1016/j.actaastro.2015.01.023.

[7] D.O. Caplan, B.S. Robinson, R.J. Murphy, M.L. Stevens, Demonstration of 2.5-gslot/s optically-preamplified M-PPM with 4 photons/bit receiver sensitivity, in: Optical Fiber Communication Conference and Exposition and the National Fiber Optic Engineers Conference, Optical Society of America, 2005, p. PDP32, http://dx.doi.org/10.1109/OFC.2005.193210.

[8] M.L. Stevens, D.M. Boroson, A simple delay-line 4-PPM demodulator with near-optimum performance, Opt. Express 20 (5) (2012) 5270–5280, http://dx.doi.org/10.1364/OE.20.005270.

[9] K. Kiasaleh, Performance of APD-based, PPM free-space optical communication systems in atmospheric turbulence, IEEE Trans. Commun. 53 (9) (2005) 1455–1461, http://dx.doi.org/10.1109/TCOMM.2005.855009.

[10] S.G. Wilson, M. Brandt-Pearce, Q. Cao, J.H. Leveque, Free-space optical MIMO transmission with Q-ary PPM, IEEE Trans. Commun. 53 (8) (2005) 1402–1412, http://dx.doi.org/10.1109/TCOMM.2005.852836.

[11] N. Letzepis, I. Holland, W. Cowley, The Gaussian free space optical MIMO channel with Q-ary pulse position modulation, IEEE Trans. Wireless Commun. 7 (5) (2008) 1744–1753, http://dx.doi.org/10.1109/TWC.2008.061002.

[12] W. Gappmair, Novel results on pulse-position modulation performance for terrestrial free-space optical links impaired by turbulent atmosphere and pointing errors, IET Commun. 6 (2012) 1300–1305, http://dx.doi.org/10.1049/iet-com.2011.0545, (5).

[13] G. Xu, Error performance of deep space optical communication with M-ary pulse position modulation over coronal turbulence channels, Opt. Express 27 (9) (2019) 13344–13356, http://dx.doi.org/10.1364/OE.27.013344.

[14] P.A. Humblet, M. Azizoglu, On the bit error rate of lightwave systems with optical amplifiers, J. Lightwave Technol. 9 (11) (1991) 1576–1582, http://dx.doi.org/10.1109/50.97649.

[15] A. Aladeloba, Performance evaluation of optically preamplified digital pulse position modulation turbulent free-space optical communication systems, IET Optoelectron. 6 (2012) 66–74, http://dx.doi.org/10.1049/iet-opt.2011.0029, (8).

[16] K. Yiannopoulos, N.C. Sagias, A.C. Boucouvalas, Average error probability of an optically pre-amplified pulse-position modulation multichannel receiver under malaga-M fading, Appl. Sci. 10 (3) (2020) http://dx.doi.org/10.3390/app10031141.

[17] J. Perina, Superposition of coherent and incoherent fields, Phys. Lett. A 24 (6) (1967) 333–334, http://dx.doi.org/10.1016/0375-9601(67)90612-3.

[18] M. Razavi, J.H. Shapiro, Wireless optical communications via diversity reception and optical preamplification, 2005, pp. 975–983, http://dx.doi.org/10.1109/TWC.2005.847102, 4 (3).

[19] K. Yiannopoulos, N.C. Sagias, A.C. Boucouvalas, On the photon counting error probability and its application in optical wireless communications, Phys. Commun. 36 (2019) 100756, http://dx.doi.org/10.1016/j.phycom.2019.100756.

[20] I.S. Gradshteyn, I.M. Ryzhik, Table of Integrals, Series, and Products, seventh ed., Elsevier/Academic Press, Amsterdam, 2007, xlviii+1171.

[21] S.S. Muhammad, T. Javornik, I. Jelovcan, Z. Ghassemlooy, E. Leitgeb, Comparison of hard-decision and soft-decision channel coded M-ary PPM performance over free space optical links, Eur. Trans. Telecommun. 20 (8) (2009) 746–757, http://dx.doi.org/10.1002/ett.1343.

[22] J. Hamkins, B. Moision, Multipulse Pulse-Position Modulation on Discrete Memoryless Channels, The Interplanetary Network Progress Report, 42–161, 2005, pp. 1–13, https://ipnpr.jpl.nasa.gov/progress_report/42-161/161I.pdf.

[23] A. Jurado-Navas, J.M. Garrido-Balsells, J.F. Paris, A. Puerta-Notario, A unifying statistical model for atmospheric optical scintillation, in: J. Awrejcewicz (Ed.), Numerical Simulations of Physical and Engineering Processes, IntechOpen, Rijeka, 2011, http://dx.doi.org/10.5772/25097.

[24] A. Al-Habash, L.C. Andrews, R.L. Phillips, Mathematical model for the irradiance probability density function of a laser beam propagating through turbulent media, Opt. Eng. 40 (8) (2001) 1554–1562, http://dx.doi.org/10.1117/1.1386641.

[25] L.C. Andrews, R.L. Phillips, Laser Beam Propagation Through Random Media, second ed., SPIE Press, Bellingham, Washington, 2005, http://dx.doi.org/10.1117/3.626196.

[26] K. Yiannopoulos, N.C. Sagias, A.C. Boucouvalas, K. Peppas, Optimal combining for optical wireless systems with amplification: The χ^2 noise regime, IEEE Photonics Technol. Lett. 30 (1) (2018) 119–122, http://dx.doi.org/10.1109/LPT.2017.2777908.

[27] S. Eger, Some elementary congruences for the number of weighted integer compositions, J. Integer Seq. 18 (4) (2015) 15.4.1 1–18.

[28] A.A. Farid, S. Hranilovic, Outage capacity optimization for free-space optical links with pointing errors, J. Lightwave Technol. 25 (7) (2007) 1702–1710, http://dx.doi.org/10.1109/JLT.2007.899174.

[29] R. Boluda-Ruiz, A. García-Zambrana, C. Castillo-Vázquez, B. Castillo-Vázquez, Novel approximation of misalignment fading modeled by beckmann distribution on free-space optical links, Opt. Express 24 (20) (2016) 22635–22649, http://dx.doi.org/10.1364/OE.24.022635.

[30] A. Jurado-Navas, J.M. Garrido-Balsells, J.F. Paris, M. Castillo-Vázquez, A. Puerta-Notario, Impact of pointing errors on the performance of generalized atmospheric optical channels, Opt. Express 20 (11) (2012) 12550–12562, http://dx.doi.org/10.1364/OE.20.012550.

Konstantinos Yiannopoulos received the Diploma and Ph.D. in Electrical and Computer Engineering at 2000 and 2004, respectively, from the School of Electrical and Computer Engineering of the National Technical University of Athens, Greece.

Dr. Yiannopoulos is an Assistant Professor at the University of Peloponnese, Greece. He was a member of the research teams of the Photonics Communications Research Laboratory at the National Technical University of Athens, Greece, from 2000 to 2004, and the Computer Networks Laboratory at the University of Patras, Greece, from 2005 to 2010. During this period, he conducted research on physical layer (optical signal processing, ultrafast optical sources, all-optical logic) and network layer (optical packet and burst switching networks) aspects of optical networks. At the present time, he is conducting research that focuses on optical wireless systems and networks.

Dr. Yiannopoulos has more than 70 published papers in international journals and conferences. His research work was granted with the "IEEE/LEOS Graduate Student Fellowship Program 2004" award and has received more than 1200 citations.

Nikos C. Sagias was born in Athens, Greece in 1974. He received the B.Sc. degree from the department of Physics (DoP) of the University of Athens (UoA), Greece in 1998. The M.Sc. and Ph.D. degrees in Telecommunication Engineering were received both from the UoA in 2000 and 2005, respectively. Since 2001, he has been involved in various National and European Research & Development projects for the Institute of Space Applications and Remote Sensing of the National Observatory of Athens, Greece. During 2006–2008, was a Postdoc research scholar at the Institute of Informatics and Telecommunications at the National Centre for Scientific Research-"Demokritos", Athens, Greece. During 2008–14 we was an Assistant Professor in the Department of Informatics & Telecommunications at the University of Peloponnese, in Tripolis, Greece, where currently is a Professor. Between 2014–16 he served as the Head of DIT.

Dr. Sagias research interests span the broad area of digital communications, and more specifically include MIMO and cooperative systems, fading channels, satellite communications and optical-wireless communication systems. In his record, he has over fifty (50) papers in prestigious international journals and more than thirty (30) in the proceedings of world recognized conferences. For five (5) years (between 2009–14) he was an Associate Editor of IEEE Transactions on Wireless Communications, while before 2009 he had served as an Editor for AEÜ International Journal of Electronics and Communications and IETE Technical Review. Additionally, he is serving as a reviewer and TPC member for various IEEE conferences (GLOBECOM, ICC, VTC, etc.). He is a co-recipient of the best paper award in communications in the IEEE Wireless Communications and Networking Conference (WCNC), Istanbul, Turkey, May 2014 and 3rd International Symposium on Communications, Control and Signal Processing (ISCCSP), Malta, March 2008. He is a senior member of the IEEE and IEEE Communications Society as well as the Hellenic Physicists Association.

Anthony C. Boucouvalas received the B.Sc. degree in Electrical and Electronic Engineering from Newcastle upon Tyne University, Newcastle, U.K., in 1978, the M.Sc. and D.I.C. degrees in Communications Engineering from Imperial College, University of London, London, U.K., in 1979, and the Ph.D. degree in fiber optics from Imperial College, in 1982. Subsequently, he joined the GEC Hirst Research Center and became Group Leader and Divisional Chief Scientist working on fiber-optic components, measurements, and sensors until 1987, when he joined Hewlett Packard Laboratories (HP) as a Project Manager. At HP, he worked in the areas of optical communication systems, optical networks, and instrumentation, until 1994, when he joined Bournemouth University, Bournemouth, U.K. In 1996, he became a Professor in Multimedia Communications, and in 1999 he became Director of the Microelectronics and Multimedia research Center. His research interests spanned the fields of wireless communications, optical fiber communications and components, multimedia communications, and human–computer interfaces where he has published over 250 papers. He has contributed to the formation of IrDA as an industry standard and he was a member of the IrDA Architectures Council contributing on new IrDA standards.

Dr. Boucouvalas was a Fellow of the Royal Society for the encouragement of Arts, Manufacturers and Commerce, Fellow of Institute of Electrical Engineers (IEE) and, in 2002, became Fellow of IEEE, for contributions to Optical fiber components and optical wireless communications. He was a Member of the New York Academy of Sciences and ACM. He was an Editor of the IEEE Wireless Communications Magazine, IEEE Transactions on Wireless Networks, Associate Editorial Member for the Wireless Communications and Mobile Computing Journal and Vice Chairman of the IEEE UK&RI Communications Chapter. He was in the Organizing Committee of the International Symposium on Communication Systems Networks and Digital Signal Processing, (CSNDSP), and a member of Technical Committees in numerous conferences.